

DETC2011-48602

**DESIGN OF AN ELECTROMAGNETIC ACTUATOR SUITABLE FOR PRODUCTION
BY RAPID PROTOTYPING**

**Matthew S. Moses
Gregory S. Chirikjian**
Department of Mechanical Engineering
Johns Hopkins University
Baltimore, MD 21218
Email: {matt.moses, gregc}@jhu.edu

ABSTRACT

This paper presents a design for an electric motor that can potentially be produced by a personal 3D printer. The concept of a Cyclic Fabrication System - a network of tools, machines, and processes capable of producing all of its constituent components - is discussed in order to provide context for the various factors influencing the design. The motor is an axial-airgap permanent-magnet motor with a flat 2-layer coil. The coil pattern makes minimal use of crossovers or vias, and is well-suited to several methods for fabricating conductive structures that are currently under development. A versatile MATLAB script is presented which is used to generate the coil pattern. Coil geometry is controlled parametrically, and it is straightforward to generate a wide variety of coils, corresponding to different arrangements of magnets and desired coil spacings. The motor uses plastic roller bearings that are easily fabricated.

INTRODUCTION

The new field of “open-source-hardware” is currently undergoing rapid development, fueled by the growing availability of personal 3D printing machines, along with convenient internet-based platforms for sharing CAD/CAM design files [1] [2]. Most personal 3D printers are limited to a few basic materials and produce parts that, while functional, are relatively crude by current industry standards. Some printers can manufacture a significant portion of their own components, but so far all of them rely on

commercially produced motors, bearings, and electronic components. A personal 3D printer capable of producing its own motors and bearings could have many advantages. This would obviously increase the availability of personal printers and the class of objects they can construct, but it could also potentially enable a greatly accelerated rate of development, since a “seed” machine would contain much of the necessary manufacturing power to produce a modified or improved version of itself. Such a machine, a self-replicating universal constructor, could have many applications ranging from space-based manufacturing to desktop manufacturing to sustainable development and nanotechnology [3].

A useful concept related to self-replicating universal constructors is a cyclic fabrication system (CFS): a network of tools, machines, and processes capable of producing all of its constituent components. The concept of a CFS provides context for the motivation to build the motor described here. The motor is a variant of well-established design; it does not perform better than commercially available motors of similar size. The novel contribution, however, is in the way it is built. Although it was not actually built on a personal 3D printer, it represents a significant step toward an actuator that *could* be fabricated on such a machine. Development of such actuators is a crucial step in developing a fully functional CFS.

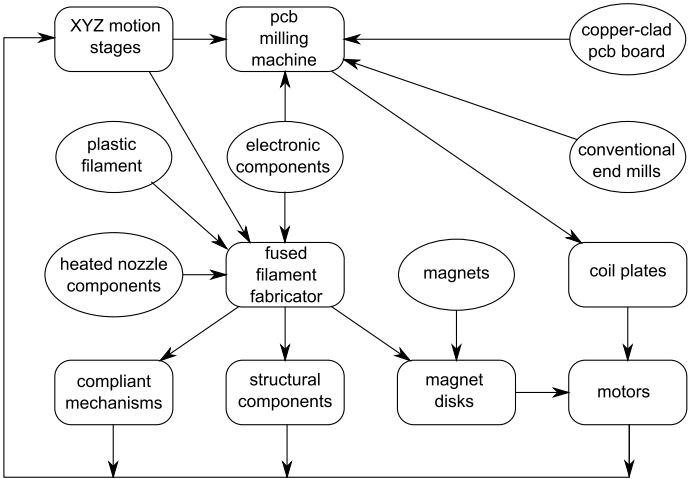


FIGURE 1. MATERIALS, TOOLS, AND MANUFACTURING PROCESSES COMprise A CYCLIC FABRICATION SYSTEM. THE SYSTEM CAN PRODUCE MOST OF ITS NECESSARY COMPONENTS.

CYCLIC FABRICATION SYSTEMS

A CFS is cyclic in the way the game “rock-paper-scissors” is cyclic: tools, materials, and fabrication processes are chosen such that one process creates tools used in the next process, which is used in the next, and so on until a final process produces tools needed to perform the initial process. Complex CFSs have been proposed in the context of self-replicating machines. Processes for producing machine components from lunar soil are proposed in [4] and [5]. A cyclic process for separating common terrestrial soil into useful materials is proposed in [6]. A proposed system outlined in [7] is based on UV-catalyzed polymer resin and fluidic control components, and [8] presents demonstrations of many solid-freeform fabrication processes that could form the core of a “compact factory”.

One proposed cyclic fabrication system that could incorporate the motor in the present paper is shown in Figure 1. Fused filament fabrication (FFF) is used to construct mechanical components (such as gears and roller bearings) from thermoplastic filament, while circuit boards and motor coils are formed by conventional milling of copper-clad insulating board. Both FFF and circuit-milling are performed with automated XYZ motion stages. The motion stages themselves can be fabricated entirely from plastic using compliant mechanisms [9], or almost entirely from plastic using mechanical linkages [10]. It is assumed that the control signals for operating the machinery within the CFS originate from an external control computer. The feedstock materials and other “vitamins” (parts that cannot be made within the CFS network) are drawn as ellipses in Figure 1.

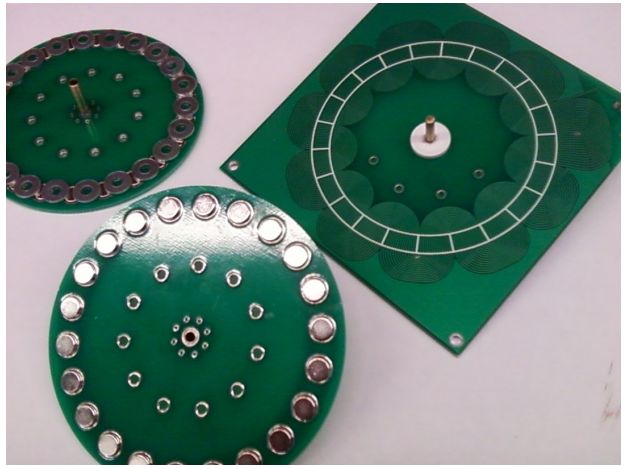


FIGURE 2. THE AXIAL AIRGAP MOTOR CONSISTS OF A COIL PLATE AND TWO MAGNET PLATES.

AXIAL AIRGAP MOTOR

Figure 2 shows a picture of the motor components. Axial airgap motors with printed coils have been built before, for example [11] [12]. The novelty in this design is that it is directed toward manufacturing by a personal 3D printer. In an earlier paper [13] we demonstrated a motor based on elements of a CFS somewhat different to that in Figure 1. The overall design of the present motor is similar to the one presented in [13], except that the coil and magnets plates are produced by commercial printed circuit board (PCB) manufacturing methods, rather than built from individual castings. The goal of this project was to dramatically increase the performance over the motor in [13] while maintaining a design that was within reach of the capabilities of a personal 3D printer. Some of the methods that could be used to produce this motor on a personal printer include etching or milling conventional PCB material, wire deposition [14], or low-melt-alloy deposition [8], all of which have been demonstrated on RepRap or Fab-At-Home personal printers.

There are three main parts to the motor - a two-sided coil plate, and two magnet disks. The coil plate is a standard 2-layer PCB; 1oz copper and 0.06 inch thick. The motor has 22 magnets, 15 turns, a trace width of 0.015 inch and a space between traces of 0.010 inch. The magnet disk has 22 magnets, each 0.25Dia × 0.125 inch, and an overall diameter of 3.5 inch. The magnet disks are made of the same PCB material as the coil plate, although they could also be laser-cut plastic or printed plastic made by FFF. The magnets are arranged in alternating polarity around the disk. Small steel washers are used to help align the magnets and also as a path for magnetic flux. The magnets are held in place by epoxy. A loose fitting axle soldered to the coil plate fits through a central hole in each magnet disk. The axle is made of brass tubing for convenience, but it could be replaced by plastic components. The disks are pulled together with a very high force

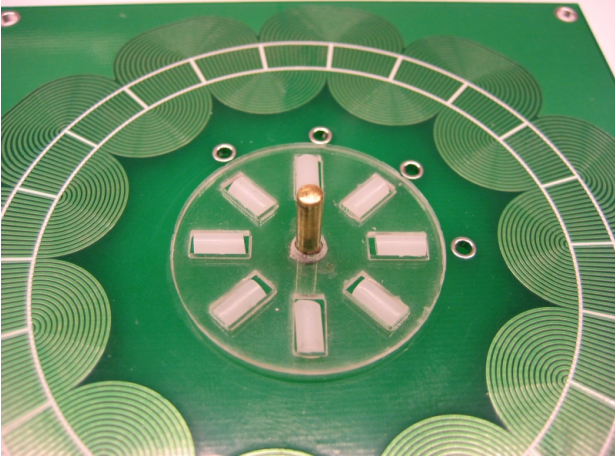


FIGURE 3. THRUST BEARINGS ARE MADE FROM A LASER-CUT PLASTIC CAGE AND EIGHT ROLLERS MADE OF 1/8 INCH DIAMETER HDPE FILAMENT.

of attraction, so thrust bearings are necessary to keep the disks apart while allowing low-friction rotation. The bearings (Figure 3) are made with a laser-cut plastic cage and rollers made of 1/8 inch diameter HDPE plastic filament. This material is chosen because it is a common feedstock for personal 3D printers and is therefore readily available. The axle, cage, and rollers could all be produced via processes within the CFS in Figure 1.

Coil Pattern

The motor needs at least two coils to operate. The coils are driven 90 degrees out of phase in a standard quadrature pattern. Multiple coil plates and magnet disks can be stacked to obtain higher torque from a motor assembly. The coil is a spiral, serpentine winding that makes minimal use of vias. Unlike most printed coil motors, the coil path does not cross the PCB multiple times. Each coil needs one crossover, which is handled with a single manually added jumper on each side of the PCB.

An open-source MATLAB script is used to generate the coil pattern. Many different patterns can be generated, depending on the size and number of magnets and the spacing between coil traces, although in all cases the patterns are for two-coil quadrature phased motors. Design flexibility is important because it allows a user to tailor the coil design to something they are capable of producing. By spacing the coils farther apart, for example, motor performance is degraded but the coil is easier to make. The output of the script can be displayed graphically, or saved as a list of commands that are interpreted by a PCB layout program such as EAGLE. The output can easily be modified to create G-code that is commonly used to control personal printers. The output provides locations for the magnets and hole locations that can be used with opto-interruptors for optical commutation. The MAT-

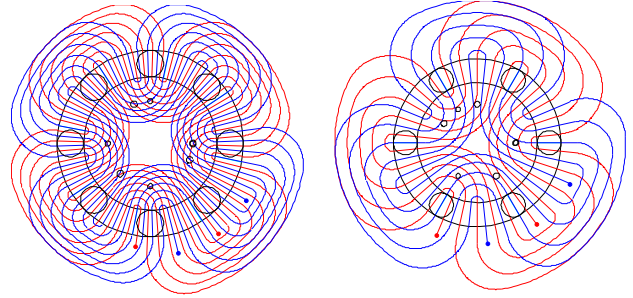


FIGURE 4. COIL PATTERNS ARE PARAMETERIZED BY NUMBER AND SIZE OF MAGNETS AND NUMBER OF TURNS. PARAMETERS CAN BE ADJUSTED TO GENERATE PATTERNS THAT ARE WITHIN THE MANUFACTURING CAPABILITIES OF A GIVEN FABRICATION SYSTEM.

LAB script also uses a simple motor model (discussed below) to predict the motor constant with reasonable accuracy, so different designs can be quickly compared. This could provide a direct interface to an evolutionary algorithm or other method for software optimization of coil geometry.

Electrical Interface

The axial motor can function as an open-loop stepper motor, or as an optically-commutated brushless DC motor. When configured as a stepper motor, the two coils are simply driven by a quadrature square wave like a standard 4-wire stepper. Performance as a stepper motor is poor. The rotor has a high inertia, which must be accelerated and decelerated each step. Performance as a brushless motor is much better because the motor is not constantly fighting the disk inertia. In brushless DC configuration, four opto-interruptors (Figure 6) are lined up with the four holes in the coil plate. As the magnet disks rotate, holes in the disks line up with one and only one hole in the coil plate. As the holes line up, the corresponding opto-interruptor is activated, which controls the energizing of one of the coils. Motor direction is reversed by switching the polarity of both coils. Opto-interruptors are used out of convenience, but they could be replaced with hall effect sensors or even electrical contacts. It is possible that a single PCB could be made which would contain the necessary coils, driver components, and sensors for an entire motor.

Motor Characterization

This section presents a simple theoretical model of the motor. Agreement between the model and experimental results is close enough that the model may be of use in designing new motors and optimizing performance using simulations. The primary parameter we are interested in is the motor constant, which serves as the constant of proportionality between back-emf and

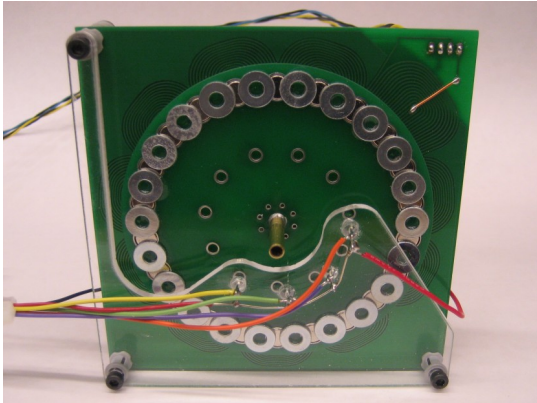


FIGURE 5. AXIAL AIRGAP MOTOR CONFIGURED WITH OPTICAL COMMUTATION.

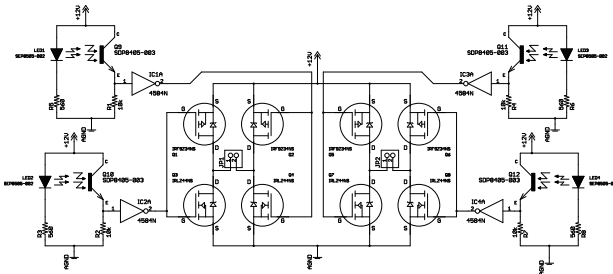


FIGURE 6. WHEN OPTICALLY COMMUTATED, THE MOTOR USES FOUR OPTO-INTERRUPTORS AND TWO H-BRIDGE DRIVERS.

speed, as well as between torque and current.

The motor produces a periodic voltage on the windings as it rotates. Likewise, given a current through the motor windings, the rotor will generate a torque that fluctuates periodically with rotor position. The torque and voltage contributions of an infinitesimal winding segment $d\vec{s}$ are given by [15]

$$d\vec{\tau} = \vec{r} \times d\vec{f} = \vec{r} \times (i(d\vec{s} \times \vec{B})) \quad (1)$$

$$dV = (\vec{v} \times \vec{B}) \cdot d\vec{s} = ((\vec{\omega} \times \vec{r}) \times \vec{B}) \cdot d\vec{s}. \quad (2)$$

The conductors are modeled as ideal line segments coincident with the centerlines of the physical conductive traces. The magnetic flux density \vec{B} is assumed to be uniform over the area of the magnets, zero outside the magnet perimeters, and directed parallel to the motor axis: $d\vec{\tau}$ and $\vec{\omega}$ are parallel with the motor axis, and \vec{r} and $d\vec{s}$ are directed radially from the axis. For these

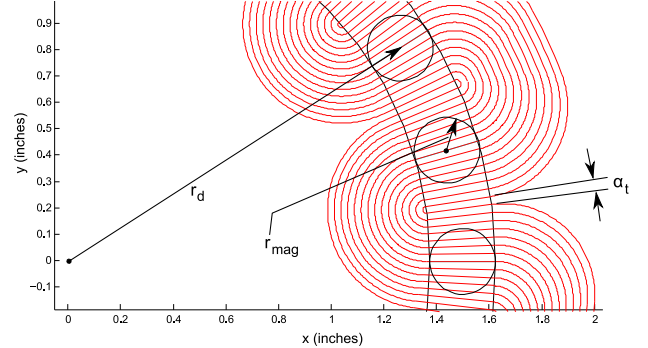


FIGURE 7. GEOMETRY FOR ESTIMATING MOTOR CONSTANT. MAGNETS ARE SHOWN BY CIRCLES. A UNIFORM FLUX DENSITY IS ASSUMED FOR EACH MAGNET.

reasons the above expressions can be simplified to the scalar expressions

$$d\tau = (Bir) dr \quad (3)$$

$$dV = (B\omega r) dr \quad (4)$$

where $\tau = \| \vec{\tau} \|$ is motor torque (Nm), $\omega = \| \vec{\omega} \|$ is angular velocity (rad/s), $r = \| \vec{r} \|$ is radial distance from center of rotation to the conductor segment (m), $B = \| \vec{B} \|$ is magnetic flux density (T), and i is the current in the conductor (A). Integrating the above quantities over all regions of conductor “underneath” the magnets results in the total torque and voltage output of the motor.

$$\tau = (2n_m Bi) \int_C r dr \quad (5)$$

$$V = (2n_m B\omega) \int_C r dr \quad (6)$$

where the domain of integration C is over the set of conductor segments within the outline of a single magnet, and n_m is the number of magnets per disk. We define the motor constant for a single coil plate, at the configuration that produces peak torque and voltage, as

$$k_M = \frac{\tau_{peak}}{i} = \frac{V_{peak}}{\omega} = (2n_m B) \int_C r dr. \quad (7)$$

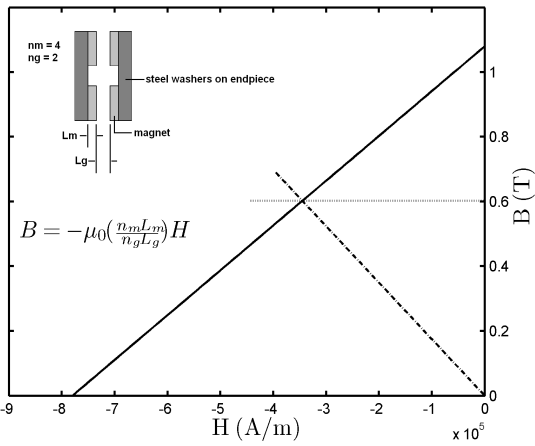


FIGURE 8. MAGNETIC FLUX DENSITY IN THE MOTOR AIR GAP IS ESTIMATED WITH A LOAD LINE AND THE DEMAGNETIZATION CURVE.

It is clear that for a single radial conductor trace directly under the center of a magnet the term $\int_C r dr$ evaluates to $2r_d r_{mag}$ (see Figure 7). Supposing the magnets are wedge-shaped (i.e. shaped like an annular sector) rather than circular, the integral over multiple conductors would then evaluate to $2r_d r_{mag} n_{tm}$. We approximate the integral for circular magnets by simply weighting the result obtained for wedges by $(\pi/4)$, as the ratio of areas between a circle and an annular sector tends to $(\pi/4)$ as $r_d/r_{mag} \rightarrow \infty$. This naive approximation yields a result for the motor constant that is very close to the measured value,

$$\int_C r dr \approx \left(\frac{\pi}{4}\right) 2r_d r_{mag} n_{tm} \quad (8)$$

where r_d is the radius to the magnet centers, r_{mag} is the radius of a magnet, and n_{tm} is approximately the number of segments “under” a magnet,

$$n_{tm} = \text{floor} \left(2 \frac{\alpha_m}{\alpha_t} \right) \quad (9)$$

where $\alpha_m = \arcsin(r_{mag}/r_d)$ is half the angle subtended by a magnet and α_t is the angular spacing between coil segments.

The magnetic flux density B in the air gap can be estimated using the method described in [16]. Geometric properties of the magnet arrangement are used to generate a “load line” which is plotted on the second quadrant of the magnetic material’s B-H curve (also known as the “demagnetization curve”). The load line is given by

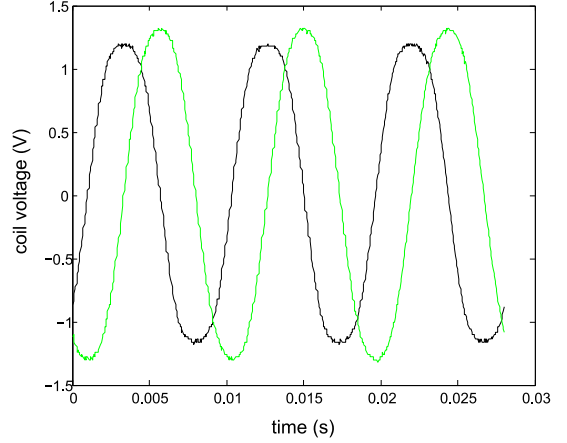


FIGURE 9. PHASE A AND PHASE B VOLTAGES WHEN MOTOR IS OPERATING AS A GENERATOR, USED TO MEASURE k_M .

$$B = -\mu_0 \left(\frac{n_{mc}L_m}{n_{gc}L_g} \right) H \quad (10)$$

where μ_0 is permeability of free space, n_{mc} and L_m are the number and thickness of the magnets in a magnetic circuit (4 and 0.0032 respectively), n_{gc} and L_g are the number and thickness of the air gaps in the magnetic circuit (2 and 0.0046m respectively), and H is the magnetic field intensity in units of A/m . The operating point of the magnet is at the intersection of the load line and demagnetization curve. In general, this requires a graphical or numeric solution because B is a nonlinear function of H . The process is somewhat simplified in the case of neodymium-iron-boron materials because the B-H curve in the second quadrant is well-approximated by a straight line [16]. Figure 8 shows a plot of the load line and demagnetization curve for the motor. The demagnetization curve is estimated from manufacturer data [17]. The steel end pieces (washers) on the magnetic assembly are assumed to be perfect conductors of magnetic flux (i.e. $\mu = \infty$). Note that, while there are 22 washers and 22 magnets per disk, it is assumed that the magnets and washers are paired such that there are eleven small magnetic circuits in the complete motor. The magnetic flux density in the air gap is estimated as $B = 0.6$ (in units of Tesla). This leads to a calculated value of the motor constant $k_M = 0.020$ in units of Vs or Nm/A . The motor constant was measured by running the motor at constant speed and measuring the generated voltages (see Figure 9). The calculated k_M is within 1% error of the measured value.

The motor can operate either as a stepper motor or an optically commutated brushless DC motor. When configured as a

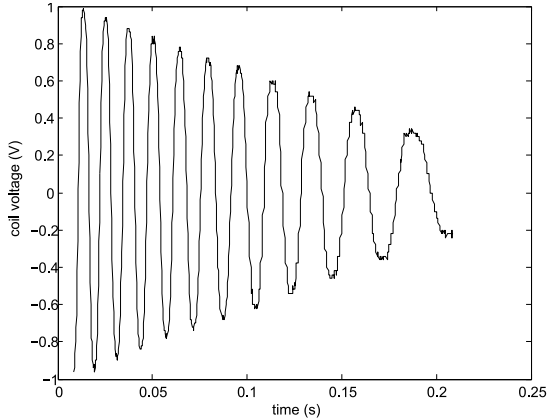


FIGURE 10. COIL VOLTAGE DURING FREE-SPINNING, USED TO ESTIMATE ROLLING FRICTION.

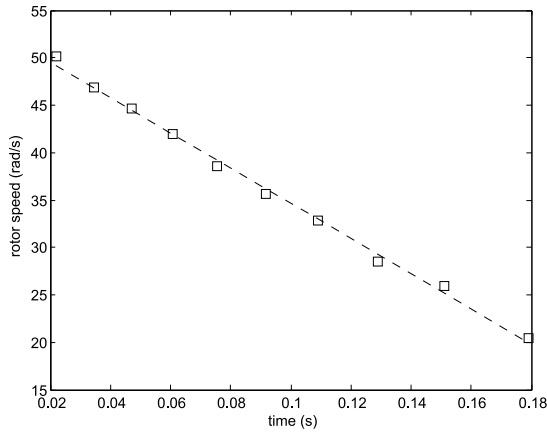


FIGURE 11. DECELERATION DUE TO FRICTION DURING FREE-SPINNING CAN BE APPROXIMATED AS A CONSTANT.

brushless motor, the optical commutator excites the coils with a quadrature square wave. It is assumed that the motor constant for DC brush operation is equal to k_M calculated for a single coil circuit. During brushless operation, both coils can actually be energized at the same time, so the true motor constant may be slightly higher than k_M . The steady-state behavior of the motor in brushless DC operation is described by

$$\tau = k_M i - \tau_f \quad (11)$$

$$i = \frac{V - k_M \omega}{R} \quad (12)$$

where τ_f is a constant torque representing sliding friction, V

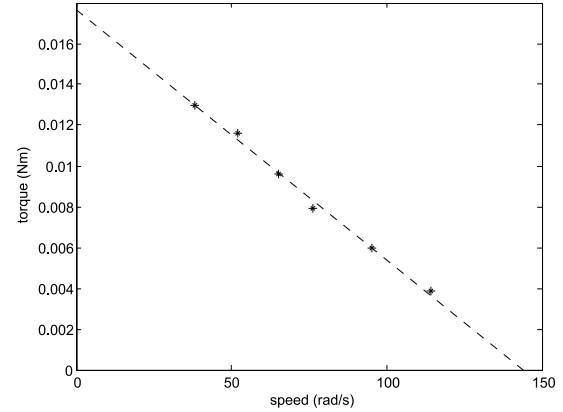


FIGURE 12. MOTOR PERFORMANCE WAS MEASURED BY LIFTING DIFFERENT WEIGHTS.

is constant DC voltage applied to the motor driver circuit, R is lumped resistance of the motor windings, and $i > \tau_f/k_M$. With some manipulation of the above it can be shown that the maximum power output of the motor is

$$P_{max} = \frac{1}{4R} \left(V - \frac{\tau_f R}{k_M} \right)^2. \quad (13)$$

Performance

The motor runs at a typical no load speed of about 228 rad/s (2180 rpm) at 12V, drawing 1.5 amps. During free-running continuous operation at a constant voltage, the motor speed can be quite variable, probably due to inconsistent friction in the bearings. Under load the speed is more consistent. Six data points were measured by using the motor to lift a weight with a pulley and string. The weight and string were simply draped over the rounded edge of a lab bench, which added an unmeasured amount of friction to the system. The weight-lifting tests were performed mainly to get a rough lower bound on the mechanical power output. The power output falls short of that predicted by the model, but it still develops enough power to perform a useful function. The power is lower than expected, in part, due to the additional unmeasured friction in the experimental setup.

CONCLUSIONS

This paper presented an electromagnetic actuator that is well-suited for production on a personal 3D printer. The design may be useful for other areas of robotics such as self-diagnosis and self-repair [18], since the modularity of the design makes it easier for a robot to handle and replace components. The axial airgap motor is strong enough that it can perform useful tasks. While this motor was produced in an industrial printed circuit facility, a similar motor could be produced using one of several

TABLE 1. AXIAL AIRGAP MOTOR PARAMETERS

Parameter	Symbol	Model	Actual	Unit
motor constant	k_M	0.020	0.020	Vs
max power at 12V	P_{max}	3.16	0.62	W
phase A resistance	R	9.8	5.2	Ω
phase B resistance	R	9.8	7.3	Ω
flux density	B	0.6	-	T
friction torque	τ_f	-	0.010	Nms
rotor inertia	J	-	5.4×10^{-5}	kgm^2
airgap	L_g	-	4.6	mm
trace width	-	-	0.38	mm
trace spacing	-	-	0.25	mm

techniques currently in development in the personal 3D printing community, such as low-melt-alloy deposition, PCB milling or etching, or wire deposition. An open-source MATLAB script was released that aids with generating flat coil patterns for axial airgap motors. The script allows a user to customize the coil pattern for manufacturability, while providing a quick way to estimate the performance of the motor. The output of the script interfaces directly to CAD/CAM software such as EAGLE PCB. The motor represents a significant improvement over our earlier attempt at a printable motor, however the design still needs to be demonstrated in a device produced on a personal printer. This is a topic for future study.

ACKNOWLEDGMENT

We acknowledge NSF Grant IIS 0915542 “Robotic Inspection, Diagnosis, and Repair” for the support of this work and Mr. Kevin Wolfe for useful discussions.

REFERENCES

- [1] Jones, R., Haufe, P., Sells, E., Iravani, P., Olliver, V., Palmer, C., and Bowyer, A., 2011. “Reprap - the replicating rapid prototyper”. *Robotica*, **29**, pp. 177–191.
- [2] Pearce, J. M., Blair, C. M., Laciak, K. J., Andrews, R., Nor-sat, A., and Zelenika-Zovko, I., 2010. “3-d printing of open source appropriate technologies for self-directed sustainable development”. *Journal of Sustainable Development*, **3**(4), December, pp. 17–29.
- [3] Freitas, R. A., and Merkle, R. C., 2004. *Kinematic Self-Replicating Machines*. Landes Bioscience.
- [4] Freitas, R. A., and Space Initiative, 1982. “Advanced automation for space missions”. In Proceedings of the 1980 NASA/ASEE Summer Study; sponsored by the National Aeronautics and Space Administration and the American Society for Engineering Education. NASA Conference Publication 2255. On-line extracts at <http://www.zyvex.com/nanotech/selfRepN>.
- [5] Chirikjian, G. S., Zhou, Y., and Suthakorn, J., 2002. “Self-replicating robots for lunar development”. *IEEE/ASME Transactions on Mechatronics*, **7**(4), pp. 462–472.
- [6] Lackner, K. S., and Wendt, C. H., 1995. “Exponential growth of large self-reproducing machine systems”. *Mathematical and Computer Modelling*, **21**(10), pp. 55–81.
- [7] Phoenix, C. J., 1998. Partial design for macro-scale machining self-replicator. <http://groups.google.com/group/sci.nanotech/msg/96a67c84809c9a5d>.
- [8] Malone, E., and Lipson, H., 2008. “Multi-material freeform fabrication of active systems”. In Proceedings of the 9th Biennial ASME Conference on Engineering Systems Design and Analysis ESDA08.
- [9] Hoover, A. M., Avadhanula, S., Groff, R. E., and Fearing, R. S., 2006. “A rapidly prototyped 2-axis positioning stage for microassembly using large displacement compliant mechanisms”. In Proceedings of the 2006 IEEE International Conference on Robotics and Automation.
- [10] Davies, F., 2009. Sarrus Linkage Mark III. online, Dec. <http://www.thingiverse.com/thing:1425>.
- [11] Koyama, H., and Haruta, Y., 1987. “Printed coil unit for small size actuator”. *US Patent 4658162*.
- [12] Hanitsch, R., Belmans, R., and Stephan, R., 1994. “Small axial flux motor with permanent magnet excitation and etched airgap winding”. *IEEE Transactions on Magnetics*, **30**(2), March, pp. 592–594.
- [13] Moses, M., Yamaguchi, H., and Chirikjian, G. S., 2009. “Towards cyclic fabrication systems for modular robotics and rapid manufacturing”. In Proceedings of Robotics: Science and Systems.
- [14] Bayless, J., Chen, M., and Dai, B., 2010. Wire embedding 3d printer. Tech. rep., University of British Columbia. http://reprap.org/mediawiki/images/2/25/SpoolHead_FinalReport.pdf.
- [15] Close, C. M., and Frederick, D. K., 1995. *Modeling and Analysis of Dynamic Systems*, second ed. John Wiley & Sons, pp. 392–396.
- [16] Fitzgerald, A. E., Kingsley, C., and Umans, S. D., 2003. *Electric Machinery*, sixth ed. McGraw-Hill, pp. 30–42.
- [17] Radial Magnet Website. Neodymium properties. <http://radialmagnet.com/neoprop2.html>.
- [18] Kutzer, M. D. M., Armand, M., Scheidt, D. H., Lin, E., and Chirikjian, G. S., 2008. “Toward cooperative team-diagnosis in multi-robot systems”. *International Journal of Robotics Research*, **27**(9), pp. 1069–1090.